Clim Dyn (2016) 46:3371–3385
DOI 10.1007/s00382-015-2773-0

Two flavors of the Indian Ocean Dipole

Satoru Endo[1] · **Tomoki Tozuka**[1]

Received: 27 April 2015 / Accepted: 17 July 2015 / Published online: 26 July 2015

Abstract The Indian Ocean Dipole (IOD) is known as a climate mode in the tropical Indian Ocean accompanied by negative (positive) sea surface temperature (SST) anomalies over the eastern (western) pole during its positive phase. However, the western pole of the IOD is not always covered totally by positive SST anomalies. For this reason, the IOD is further classified into two types in this study based on SST anomalies in the western pole. The first type (hereafter "canonical IOD") is associated with negative (positive) SST anomalies in the eastern (central to western) tropical Indian Ocean. The second type (hereafter "IOD Modoki"), on the other hand, is associated with negative SST anomalies in the eastern and western tropical Indian Ocean and positive SST anomalies in the central tropical Indian Ocean. Based on composite analyses, it is found that easterly wind anomalies cover the whole equatorial Indian Ocean in the canonical IOD, and as a result, positive rainfall anomalies are observed over East Africa. Also, due to the basin-wide easterly wind anomalies, the canonical IOD is accompanied by strong sea surface height (SSH) anomalies. In contrast, zonal wind anomalies converge in the central tropical Indian Ocean in the IOD Modoki, and no significant precipitation anomalies are found over East Africa. Also, only weak SSH anomalies are seen, because equatorial downwelling anomalies induced by westerly wind anomalies in the west are counteracted by equatorial upwelling anomalies caused by easterly wind anomalies in the east.

✉ Satoru Endo
s_endo@eps.s.u-tokyo.ac.jp

[1] Department of Earth and Planetary Science, Graduate School of Science, The University of Tokyo, 7-3-1 Hongo, Bunkyo-ku, Tokyo 113-0033, Japan

1 Introduction

Different flavors of climate modes have received more and more attentions recently. In the tropical Pacific, Ashok et al. (2007) have identified a new type of El Niño/Southern Oscillation (ENSO), which they named ENSO Modoki. In contrast to canonical El Niño with warm sea surface temperature (SST) anomalies over the eastern tropical Pacific, El Niño Modoki is associated with warm SST anomalies in the central tropical Pacific and cold SST anomalies in the western and eastern tropical Pacific. Two different flavors of ENSO attracted much attention owing to different teleconnection patterns (Weng et al. 2007) and impacts on local sea level changes (Behera and Yamagata 2010). Also, occurrence/amplitude of ENSO Modoki may increase under global warming (Yeh et al. 2009; Ashok and Yamagata 2009; Kim and Yu 2012), although the recent increase may be a part of natural variability (Yeh et al. 2011; Newman et al. 2011; McPhaden et al. 2011; Kim et al. 2012).

In contrast to the situation in the tropical Pacific, different flavors of climate modes, such as the Indian Ocean Dipole (IOD; Saji et al. 1999), have not been studied much in the tropical Indian Ocean. However, there are some studies focusing on differences in evolution of the IOD. Rao and Yamagata (2004) and Rao et al. (2009) pointed out the existence of "aborted IOD", in which the IOD was abruptly terminated by downwelling Kelvin waves generated by intraseasonal disturbances. More recently, Du et al. (2013) classified IOD events into three types based on their evolution. According to their definition, normal IOD events develop and mature mostly in boreal fall, whereas unseasonable IOD events develop and mature mostly in boreal summer and prolonged IOD events develop in boreal summer and mature in boreal fall. However, no study to date classified the IOD based on spatial patterns

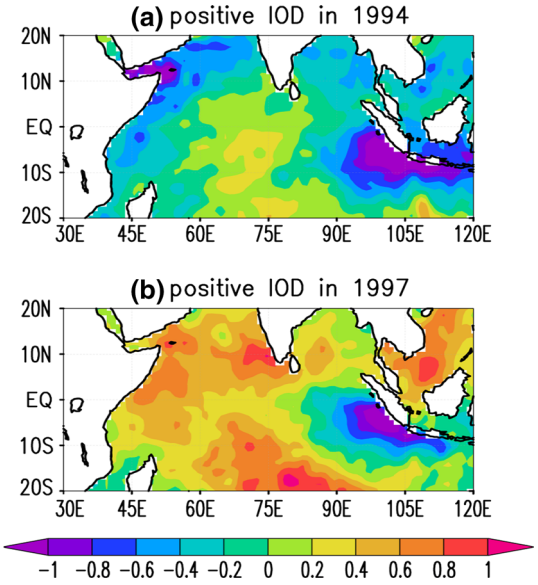

Fig. 1 SST anomalies (°C; *shading*) in the tropical Indian Ocean at the peak of the IOD events: **a** a typical IOD Modoki in August, 1994, and **b** a typical canonical IOD in October, 1997

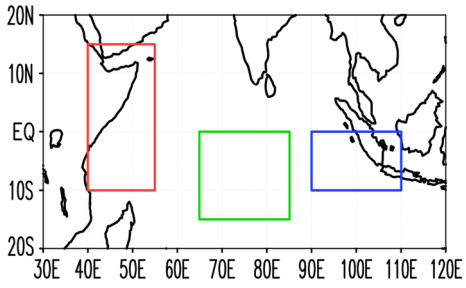

Fig. 2 Three *boxes* used to classify the two types of the IOD. *Blue*, *green*, and *red boxes* indicate the eastern (90°E–110°E, 10°S-Eq), central (65°E–85°E, 15°S-Eq), and western (40°E–55°E, 10°S–15°N) boxes, respectively

of SST anomalies. Figure 1, for example, shows SST anomalies observed at the peak phase of two major IOD events in the past few decades. Although strong negative SST anomalies are found off Sumatra both in the 1994 and 1997 events, positive (negative) SST anomalies can be found in the central Indian Ocean (off East Africa) in the former event, while

Table 1 Years of two types of the IOD from 1950 to 2012

	IOD Modoki	Canonical IOD	weak IOD Modoki
Positive IOD	1963, 1967, 1976, 1991, 1994, 2003, 2008	1961, 1972, 1982, 1987, 1997, 2011, 2012	2006
Negative IOD	1955, 1956, 1960, 1968, 1973, 1974, 1978, 1989, 1992, 1998	1958, 1980, 1996, 2010	1975, 2005

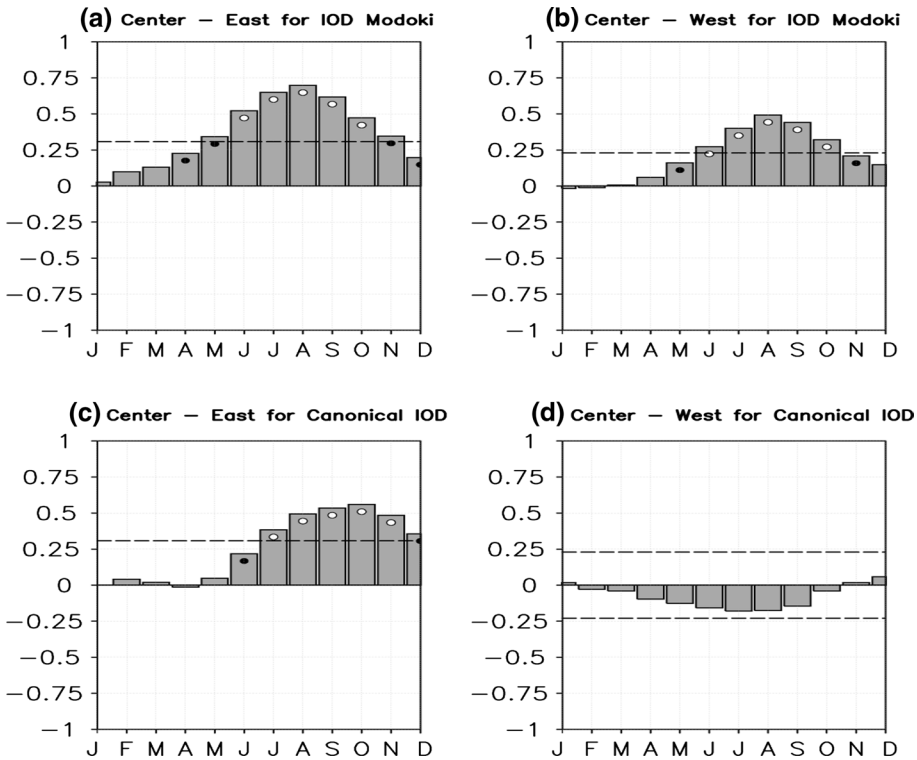

Fig. 3 **a** Time series of the difference of area-averaged SST anomalies (°C) in the central box (65°E–85°E, 15°S-Equator) and the eastern box (90°E–110°E, 10°S-Equator) for the composite of the positive IOD Modoki events. **b** As in **a**, but for the difference between the central (65°E–85°E, 15°S-Equator) and western (40°E–55°E, 10°S–15°N) boxes. **c** As in **a**, but for the composite of the positive canonical IOD events. **d** As in **b**, but for the composite of the positive canonical IOD events. *Open* and *closed circles* indicate anomalies exceeding the 99 and 95 % confidence level, respectively, by a two-tailed *t* test. *Dashed lines* represent 1 SD

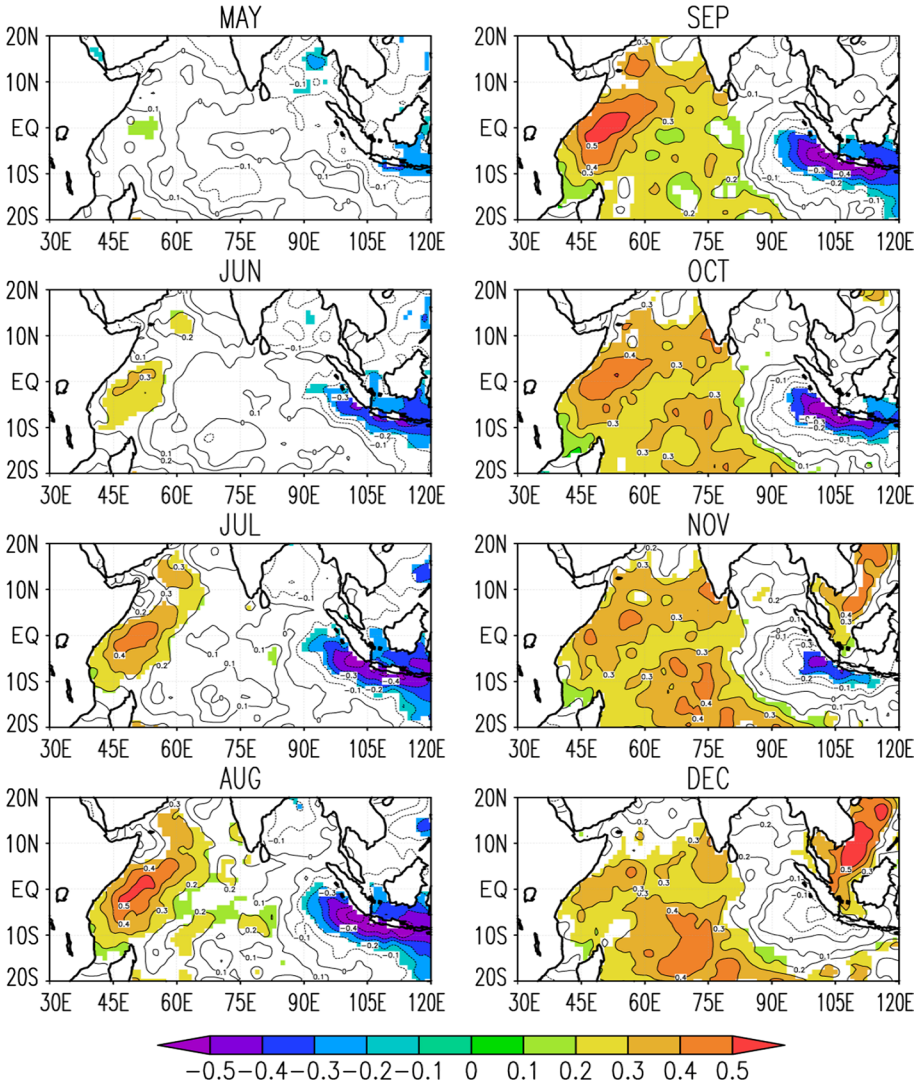

Fig. 4 Composites of SST anomalies (°C) associated with seven canonical IOD events from May to December. Contour interval is 0.1 °C and anomalies significant at the 90 % confidence level by a two-tailed *t* test are *shaded*

positive SST anomalies cover the central and western tropical Indian Ocean in the latter event. Since the IOD is known to influence precipitation over both the Indian Ocean rim countries (Behera et al. 2005; Ummenhofer et al. 2009; Cai et al. 2009; Pourasghar et al. 2012) and remote areas (Guan and Yamagata 2003; Saji and Yamagata 2003; Behera et al. 2013), differences in SST anomaly patterns may modify these climatic impacts. This is the main motive of this study.

Here, we introduce a method to identify two types of the IOD based on spatial patterns of SST anomalies and describe oceanic and atmospheric anomalies associated with each type. We also examine differences in impacts of the two types of the IOD on the tropical Indian Ocean rim countries. This study is organized as follows. A brief description of observational data and an assimilation product is given in the next section. In Sect. 3, we classify the IOD events into two types based on the difference in spatial patterns of SST anomalies. Then, we describe both types of the IOD based on composite analyses in Sect. 4. The final section summarizes the main results.

2 Data

We use SST data from the Hadley Centre Sea Ice and SST (HADISST) dataset (Rayner et al. 2003) from 1950 to

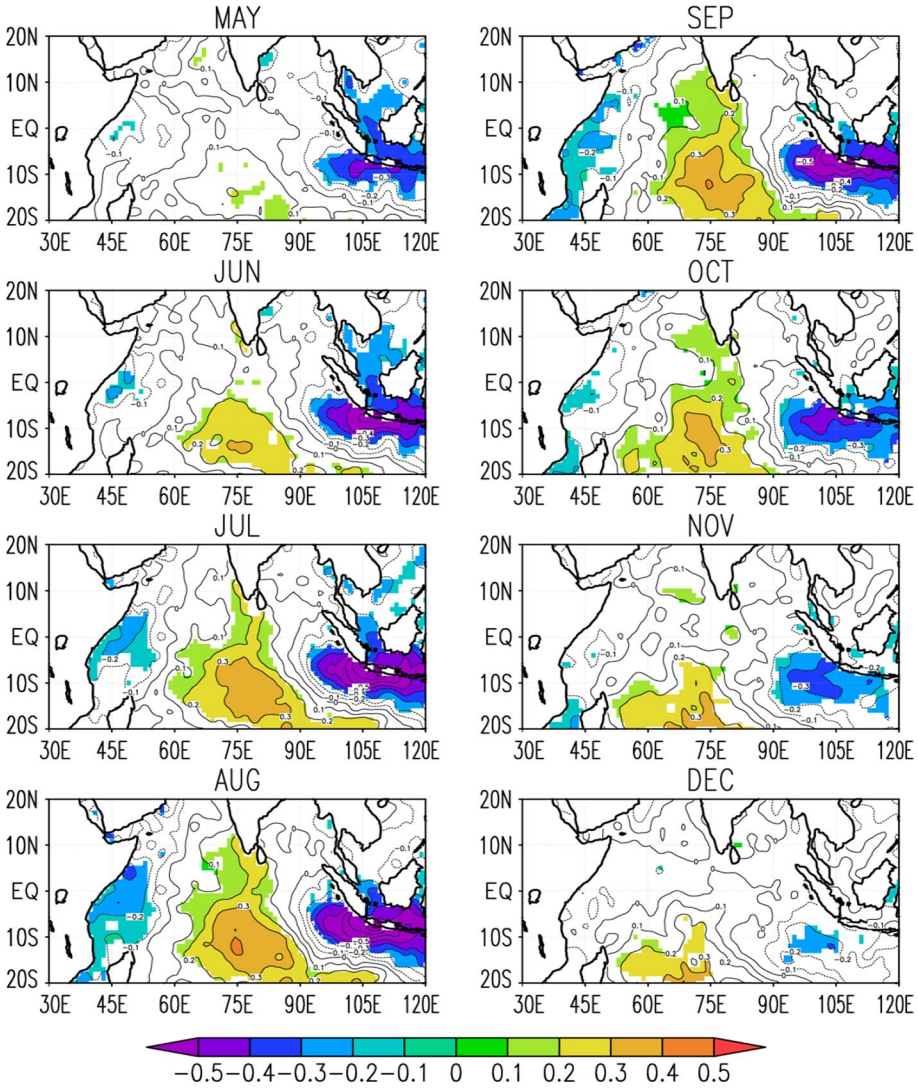

Fig. 5 As in Fig. 4, but for seven IOD Modoki events

2012. Wind data at 850 hPa from the National Centers for Environmental Prediction (NCEP) and National Center for Atmospheric Research (NCAR) reanalysis data (Kalnay et al. 1996) from 1950 to 2012, rainfall data from the Global Precipitation Climatology Project (GPCP) (Adler et al. 2003) from 1950 to 2010, sea surface height (SSH) data from the Simple Ocean Data Assimilation (SODA; Carton and Giese 2008) from 1958 to 2010, and outgoing longwave radiation (OLR) data from the National Oceanic and Atmospheric Administration (NOAA) (Liebmann and Smith 1996) from 1979 to 2012 are used. A linear trend and the monthly mean climatology are removed from each data and 3-month running mean is applied to obtain anomaly fields.

We note that our findings are qualitatively the same even if we use the Extended Reconstructed SST version3b (ERSST v3b) (Smith et al. 2008) from 1950 to 2012 for the SST, the European Centre for Medium-Range Weather Forecasts (ECMWF) 40-year Re-analysis (ERA-40) (Uppala et al. 2005) from 1958 to 2001 for the wind at 850 hPa, the Climate Prediction Center Merged Analysis of Precipitation (CMAP) (Xie and Arkin 1997) from 1979 to 2012 for the rainfall, and the NCEP Global Ocean Data

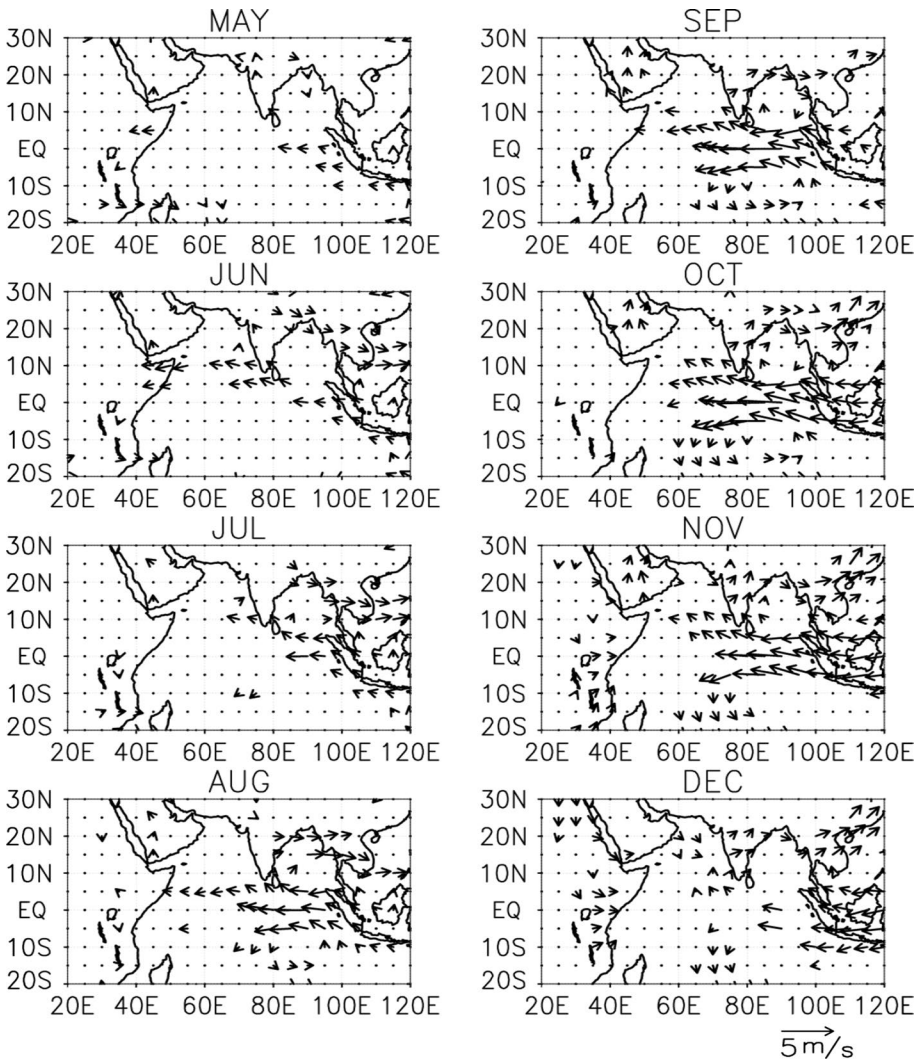

Fig. 6 As in Fig. 4, but for wind anomalies at 850 hPa (m/s; vector)

Assimilation System (GODAS) (Behringer and Xue 2004) from 1982 to 2012 for the SSH.

3 Classification method

To classify the IOD into two types based on the distribution of SST anomalies, we need to come up with a new objective method. Based on the SST anomaly patterns in 1994 and 1997 (Fig. 1), we first introduce three boxes in the eastern (90°E–110°E, 10°S-Equator), western (40°E–55°E, 10°S–15°N), and central (65°E–85°E, 15°S-Equator) tropical Indian Ocean as indicated in Fig. 2, and calculate area-averaged SST anomalies in each box. Second, we define a year as a positive (negative) IOD year if the difference in SST anomalies averaged over the central and eastern boxes is above one (below negative one) standard deviation (about 0.308 K) for at least two consecutive months between July and December. Third, we calculate the difference in SST anomalies averaged over the central and western boxes. If the difference is positive (negative) with a colder

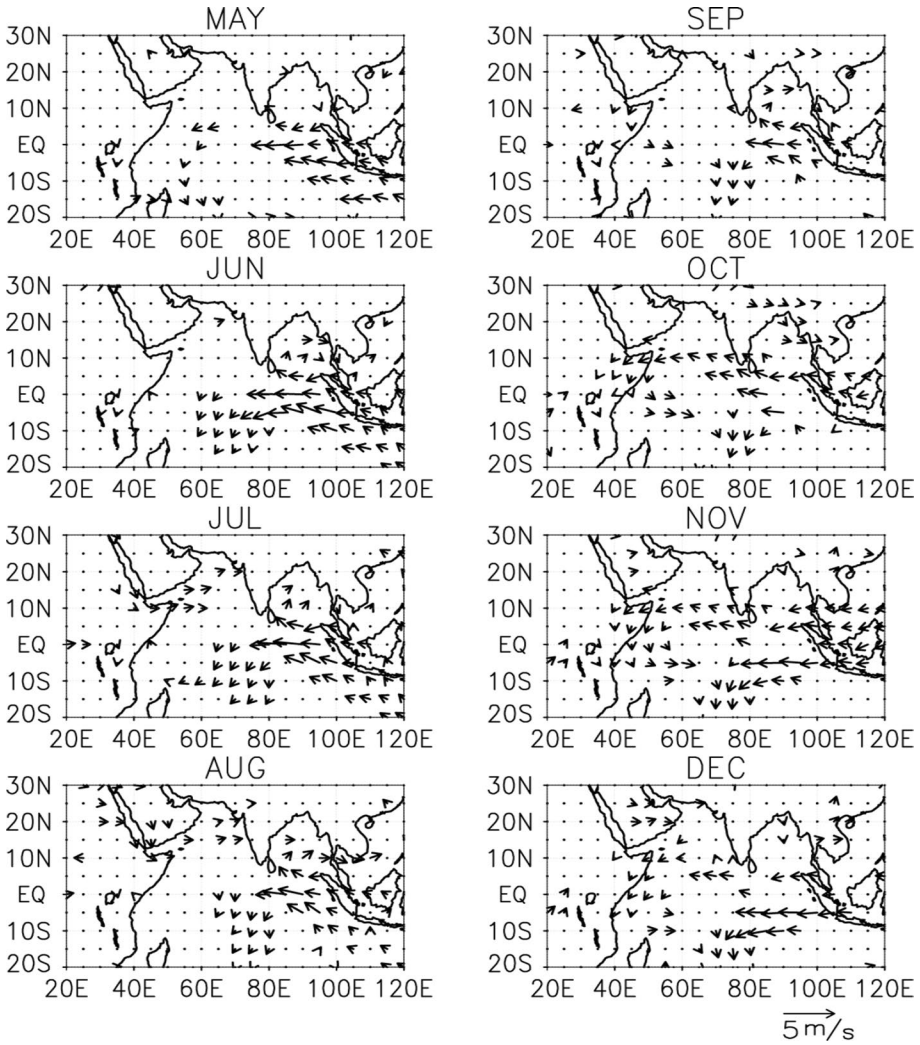

Fig. 7 As in Fig. 6, but for the IOD Modoki events

(warmer) western box and its absolute value greater than one standard deviation (about 0.229 K) for at least two consecutive months between July and December, the IOD is referred to as an "IOD Modoki" because of its similarity to the ENSO Modoki (Ashok et al. 2007) in terms of the SST anomaly pattern. If the absolute value of the difference between the central and the western boxes were between 0.5 and 1.0 standard deviation in the same period as the IOD Modoki, the IOD is referred to as a weak IOD Modoki. Other IOD years are referred to as a canonical IOD. As a result, we have seven positive (ten negative) IOD events for the IOD Modoki, seven positive (four negative) IOD events for the canonical IOD, and one positive (two negative) IOD events for the weak IOD Modoki (Table 1).

We note that our result is not very sensitive to the above definition; even if the threshold values used for the classification are slightly changed (e.g., using 1.2 standard deviation instead of 1.0 SD) or the domain of three boxes is slightly shifted, the characteristics of the two types of the IOD do not change qualitatively. Also, since the number of IOD events classified into the weak IOD Modoki is small, we do not discuss this type in the rest of this paper.

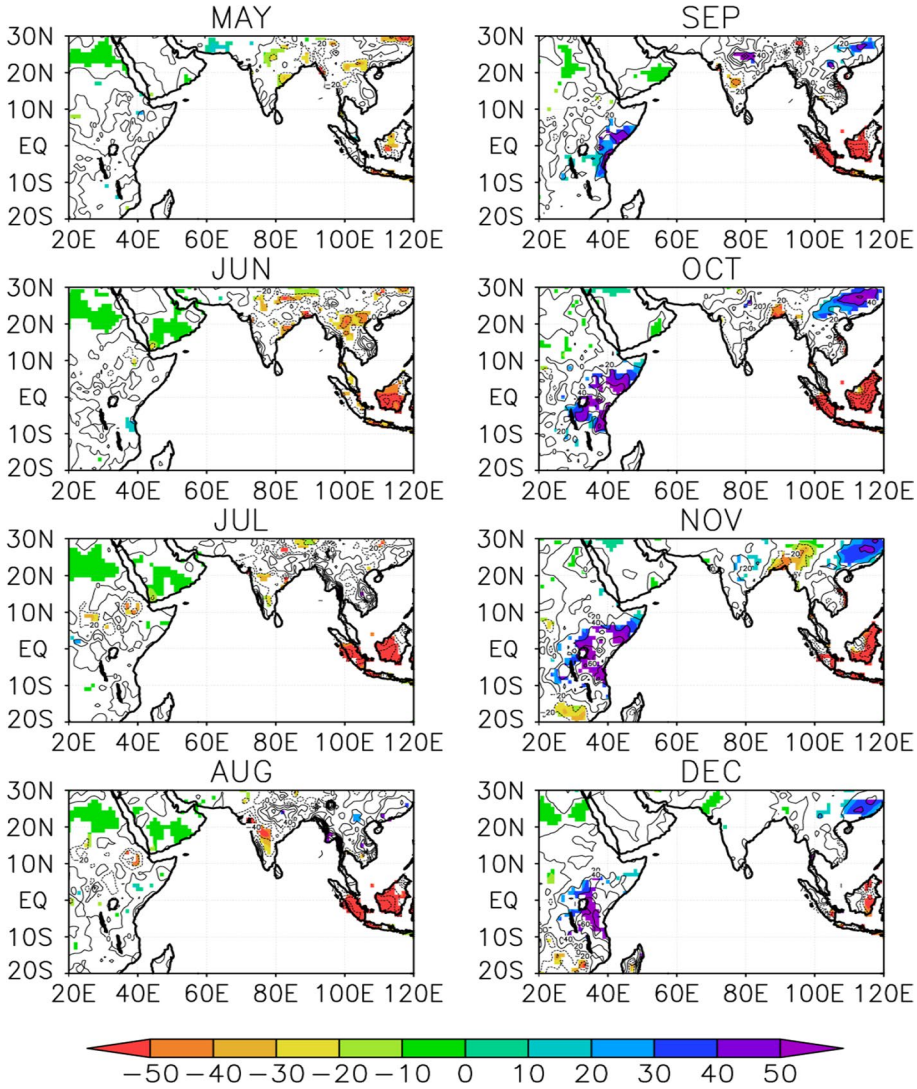

Fig. 8 As in Fig. 4, but for rainfall anomalies (mm/month) of five canonical IOD events. Contour interval is 20 mm/month and anomalies significant at the 80 % confidence level by a two-tailed *t* test are *shaded*

4 Two types of the IOD

Figure 3 shows the time-series of the composited difference in SST anomalies between the central and eastern boxes and that between the central and western boxes during the two types of the IOD events. In the IOD Modoki, the difference between the central and western boxes has the same sign with the difference between the central and eastern boxes (Fig. 3a, b), and both peak in August. In contrast, the difference between the central and eastern boxes is significantly positive with its maximum in October (Fig. 3c), but that between the central and western boxes is not significant for the canonical IOD (Fig. 3d).

The evolution of SST anomalies associated with the canonical IOD and the IOD Modoki can be compared in Figs. 4, 5. In the canonical IOD (Fig. 4), negative SST anomalies off Sumatra start to develop in May–June, reach the peak in August–September, and decay in October–December. Meanwhile, positive SST anomalies first appear off East Africa in June, develop in July–August with significant anomalies starting to appear in the central Indian Ocean around August–September and persisting

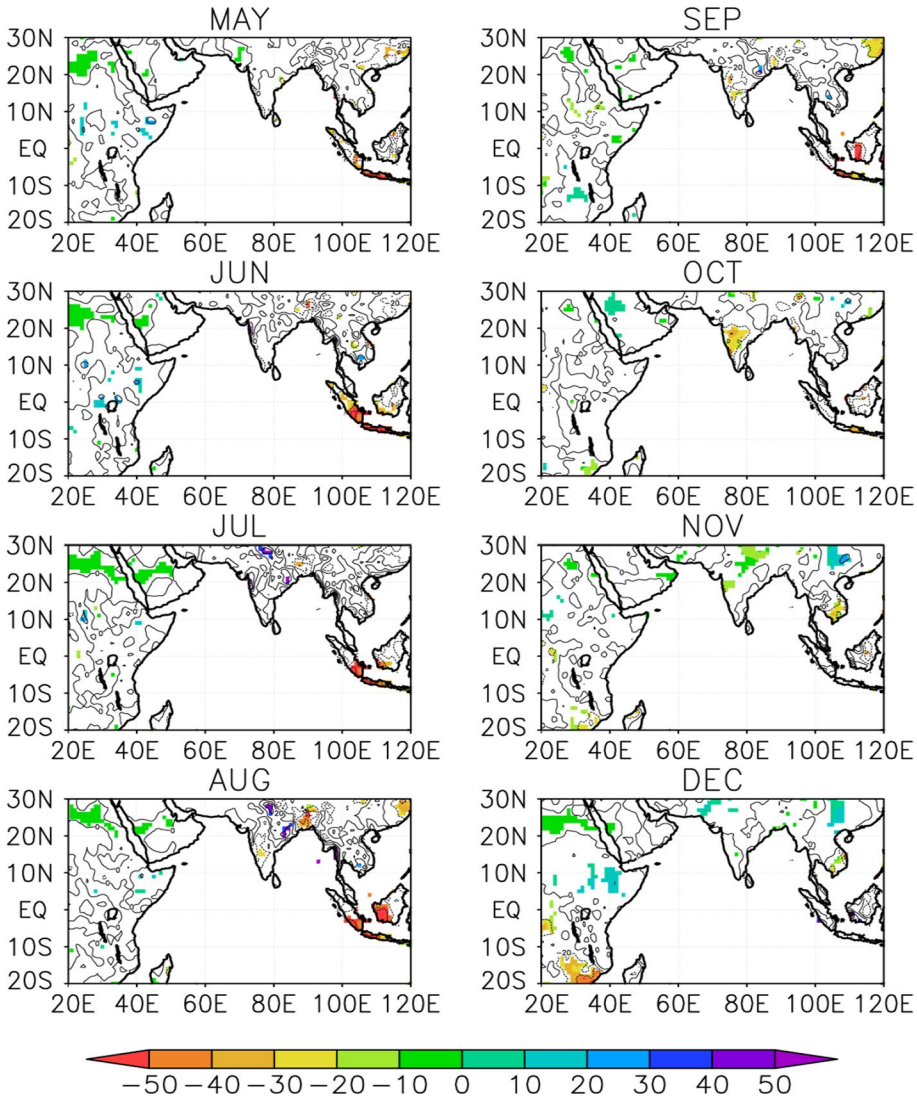

Fig. 9 As in Fig. 8, but for seven IOD Modoki events

until the end of the year. On the other hand, the IOD Modoki (Fig. 5) shows quite different evolution over the western and central tropical Indian Ocean even though negative SST anomalies off Sumatra show similar evolution. Significant negative (positive) SST anomalies first appear off East Africa (over the central Indian Ocean) in May–June. The negative SST anomalies become stronger and reach the peak in August, but decay in September–October. The positive SST anomalies persist longer than the negative SST anomalies off East Africa. We note that the amplitude in the eastern pole is stronger than that in the western and central poles for both types.

The above SST anomalies are associated with contrasting wind anomalies (Figs. 6, 7). In the canonical IOD (Fig. 6), easterly wind anomalies that favor coastal upwelling and larger latent heat loss first appear off Sumatra in June, when negative SST anomalies first appear. Easterly wind anomalies along the equator gradually extend westward and cover the whole basin in September–November, but retreat in December. In contrast, southeasterly wind anomalies off Sumatra first appear in May during the IOD Modoki, but easterly wind anomalies do not extend to the western tropical Indian Ocean like the canonical IOD (Fig. 7). In the western tropical Indian Ocean,

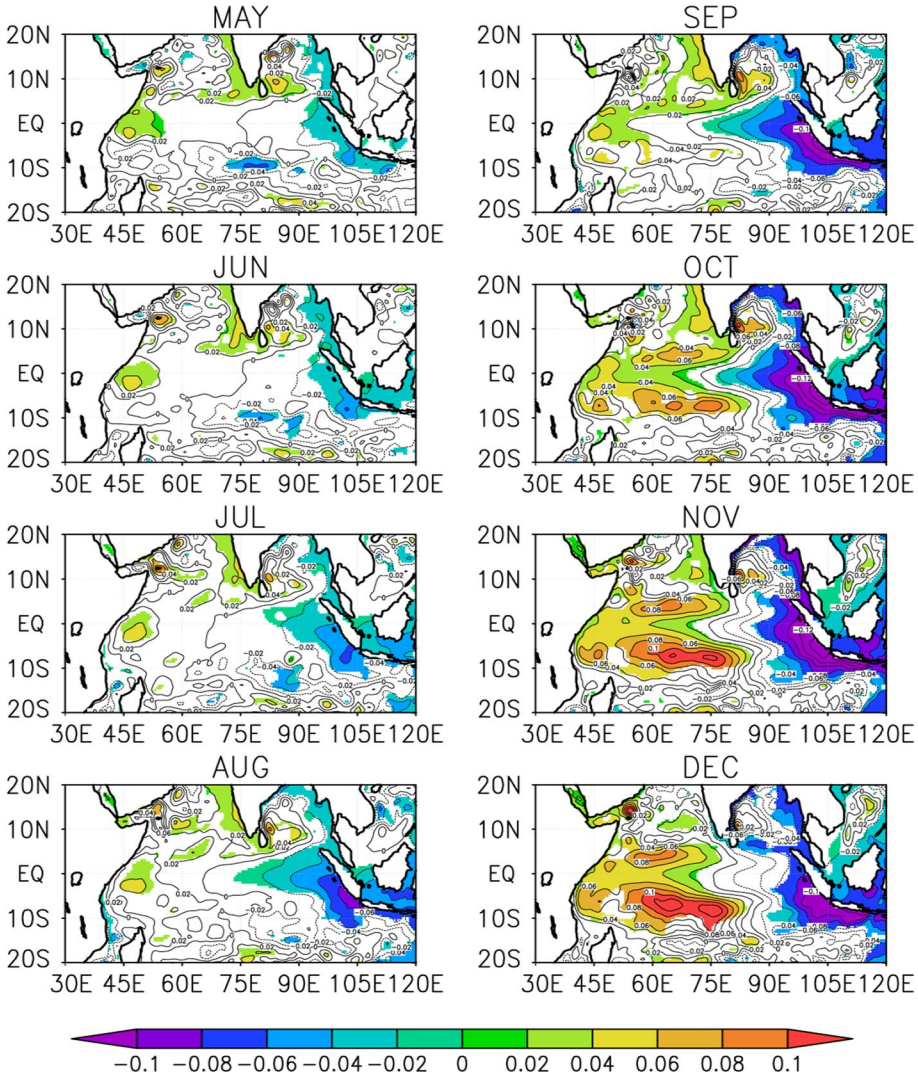

Fig. 10 As in Fig. 4, but for SSH anomalies (m) of five canonical IOD events. Contour interval is 0.02 m and anomalies significant at the 80 % confidence level by a two-tailed *t* test are shaded

northwesterly wind anomalies develop in September and westerly wind anomalies converges with the easterly wind anomalies in the central tropical Indian Ocean to the south of the equator.

Because of the large differences in SST and wind anomalies, rainfall anomalies are also quite different. In the canonical IOD, an anomalous decrease (increase) is found over the Indonesian Archipelago (East Africa) in June-December (September–December) (Fig. 8). The October–December season corresponds to the short rain season in East Africa, which is known to be strongly influenced by the IOD (Behera et al. 2005). In the IOD Modoki, on the other hand, no significant rainfall anomalies are found in the Indian Ocean rim countries, although weak negative anomalies are seen in Sumatra in boreal summer (Fig. 9). The reason for no significant rainfall anomalies especially in East Africa is that zonal wind anomalies along the equator converge in the central Indian Ocean (Fig. 7).

The above differences in wind anomalies also result in big differences in oceanic anomalies associated with the IOD, so called the "subsurface IOD" (Rao et al. 2002). Since easterly wind anomalies along the equator extend across the basin in the canonical IOD, large negative SSH anomalies associated with upwelling Kelvin

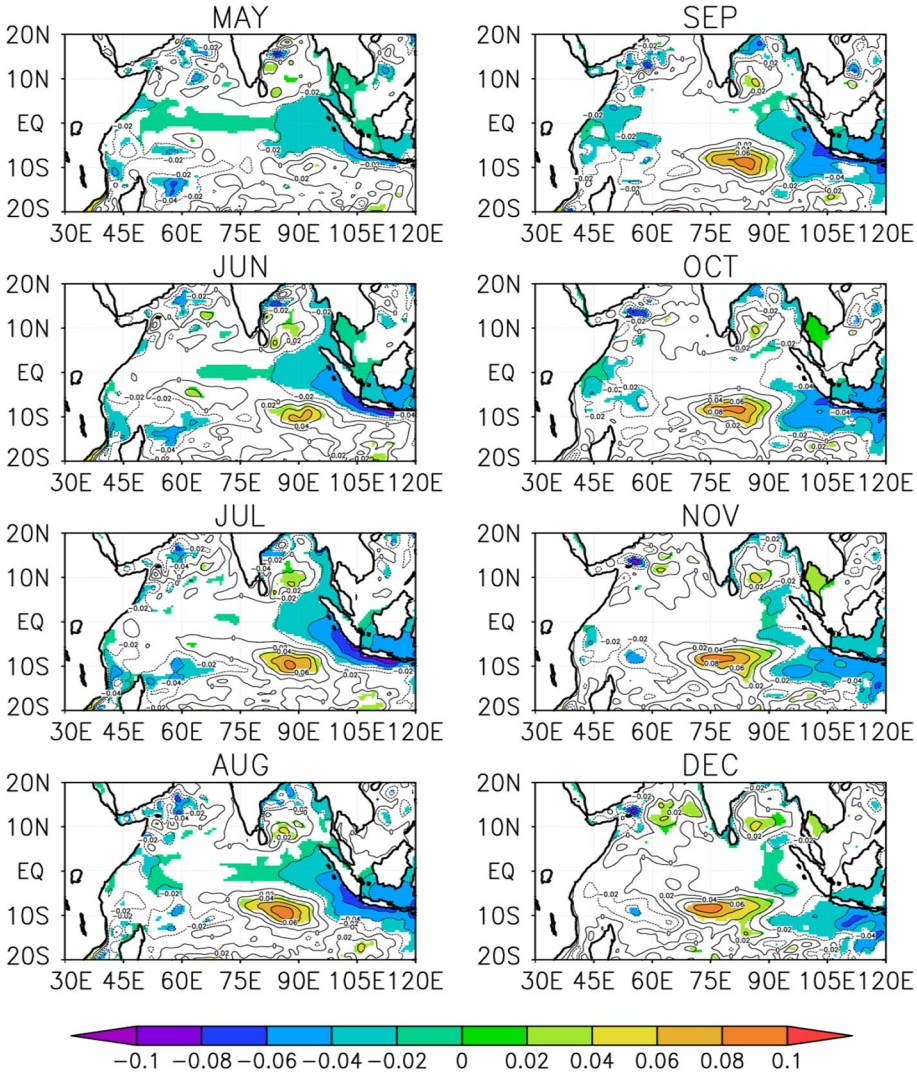

Fig. 11 As in Fig. 10, but for seven IOD Modoki events

waves are generated in the east, and large positive SSH anomalies associated with downwelling Rossby waves are generated in the west with their maxima in the off-equatorial region (Fig. 10). On the other hand, negative SSH anomalies during the IOD Modoki are weaker than the canonical IOD off Sumatra (Fig. 11). This is because equatorial upwelling anomalies caused by easterly wind anomalies in the east are counteracted by the equatorial downwelling anomalies caused by westerly wind anomalies in the west, and only weak negative SSH anomalies are found in the east. In the off-equatorial region, downwelling and upwelling Rossby waves also cancel out each other, and only weak positive SSH anomalies are found.

Despite the difference in SSH anomalies off Sumatra in boreal fall between the two types of the IOD, SST anomalies off Sumatra are not much different between these two types. This result is somewhat surprising considering that larger negative SSH anomalies imply stronger cooling associated with oceanic processes, but this can be explained by a difference in OLR anomalies. In the canonical IOD, positive OLR anomalies over the Indonesian Archipelago and off Sumatra appear in May, peak in August-October, and persist till December (Fig. 12). On the other hand, in

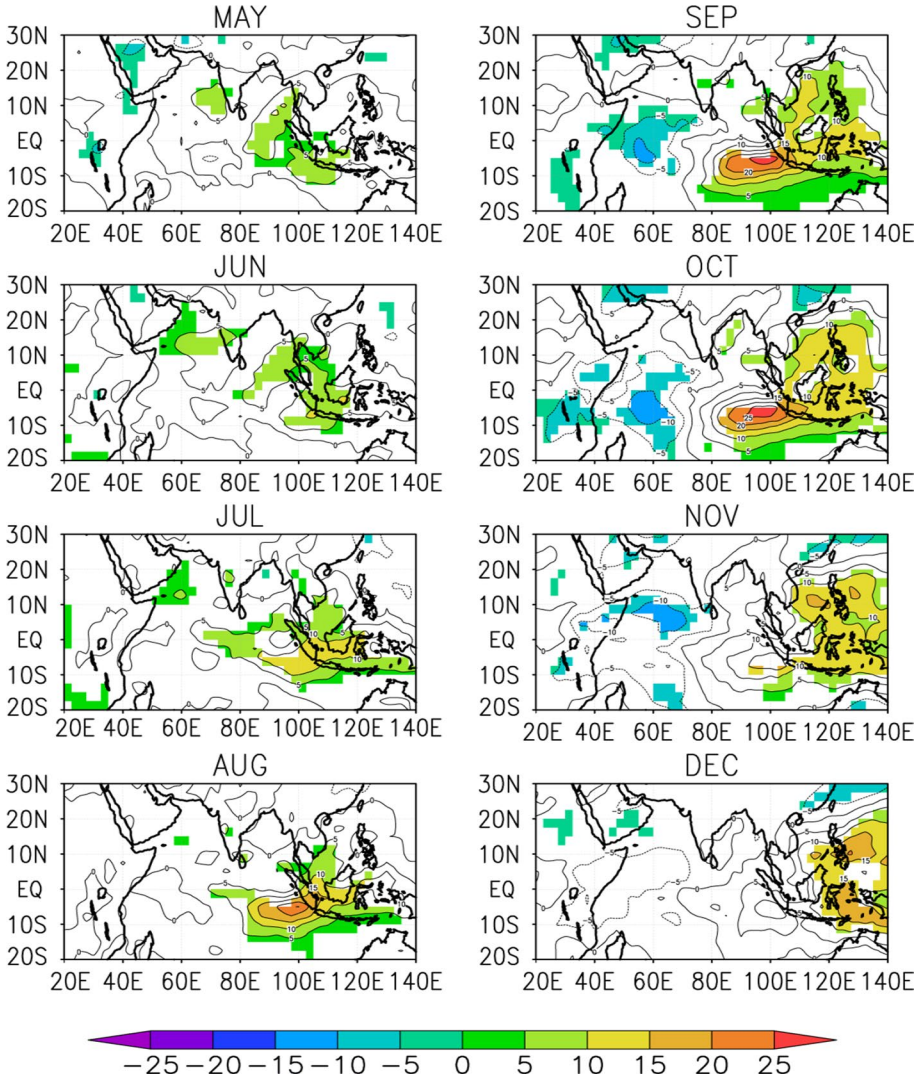

Fig. 12 As in Fig. 4, but for OLR anomalies (W/m^2) of five canonical IOD events. Contour interval is 5 W/m^2 and anomalies significant at the 80 % confidence level by a two-tailed *t* test are *shaded*

the IOD Modoki, positive OLR anomalies off Sumatra also appear in May and develop in June–August, but the anomalies decay earlier than the canonical IOD (Fig. 13). Thus, strong cooling by the oceanic processes in the eastern tropical Indian Ocean implied by the large negative SSH anomalies in the canonical IOD is counteracted by an increase in shortwave radiation reaching the ocean surface implied by the stronger and more prolonged positive OLR anomalies.

Since negative IOD events are close to a mirror image of positive events, we do not present composites of SST, wind, SSH and OLR anomalies for the sake of brevity. However, we briefly discuss rainfall anomalies associated with the two types of negative IOD events here, because precipitation anomalies have large impacts on the Indian Ocean rim countries. Figures 14 and 15 show composites of precipitation anomalies associated with negative canonical IOD and IOD Modoki events, respectively. In the negative canonical IOD, East Africa becomes anomalously dry from September to December (Fig. 14). Although precipitation anomalies last as long as those in the positive canonical IOD, the magnitude is smaller during the negative canonical IOD. On the other hand, as is the case with the positive IOD Modoki, no significant precipitation anomalies are found over East Africa during the negative IOD Modoki.

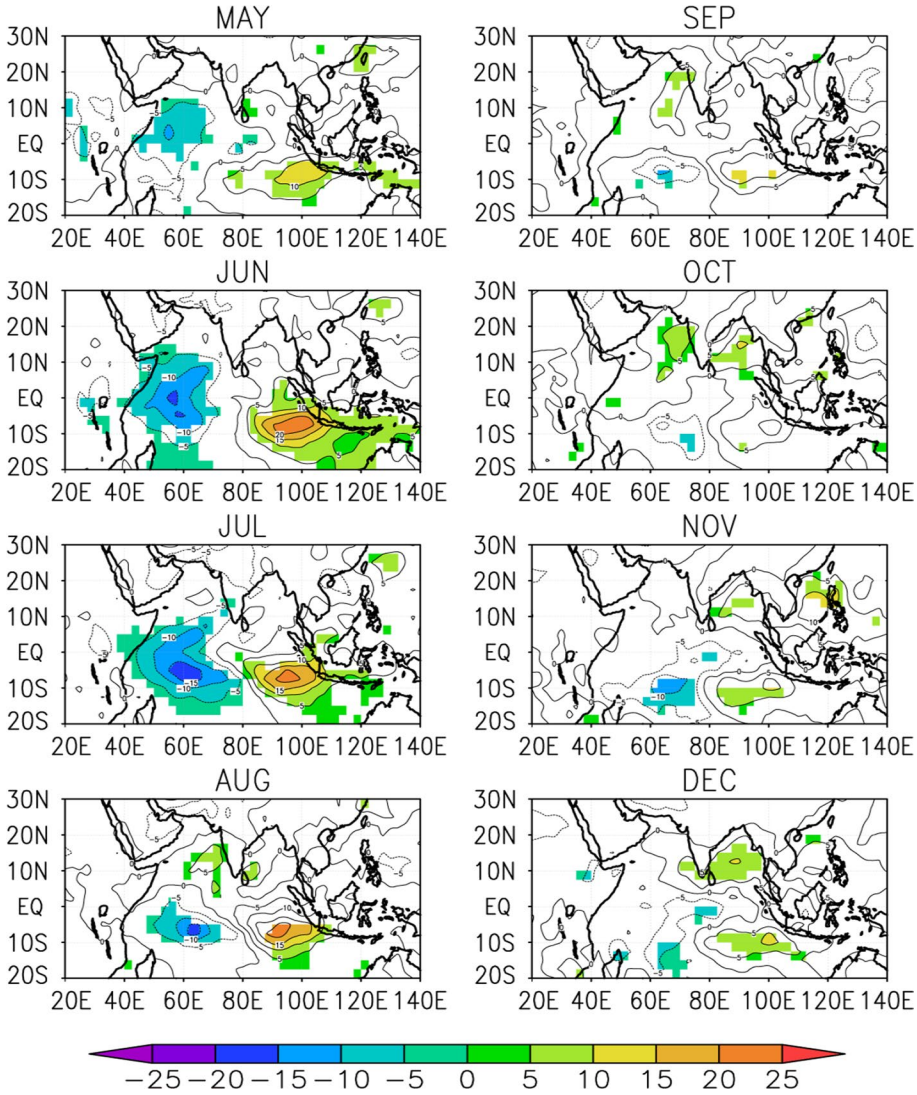

Fig. 13 As in Fig. 12, but for four IOD Modoki events

5 Conclusions

In this study, we have classified the IOD into two types (i.e. canonical IOD and IOD Modoki) based on SST anomaly patterns and compared SST, wind, rainfall, SSH, and OLR anomalies associated with them.

In the canonical IOD, negative (positive) SST anomalies cover the eastern (central and western) tropical Indian Ocean. Due to strong easterly wind anomalies across the equatorial Indian Ocean, strong negative SSH anomalies are generated in the eastern equatorial Indian Ocean. Also, positive SSH anomalies appear in the off-equatorial western Indian Ocean and it is suggested that these are associated with equatorial downwelling Rossby waves. Moreover, rainfall in East Africa increases, while that over the Indonesian Archipelago decreases.

On the other hand, in the IOD Modoki, negative SST anomalies are found over the eastern and western tropical Indian Ocean, while the central tropical Indian Ocean is covered by positive SST anomalies. Because equatorial zonal wind anomalies converge in the central tropical Indian Ocean, significant rainfall anomalies do not appear in East Africa, and SSH anomalies in the eastern equatorial Indian Ocean are weaker than those of the canonical IOD.

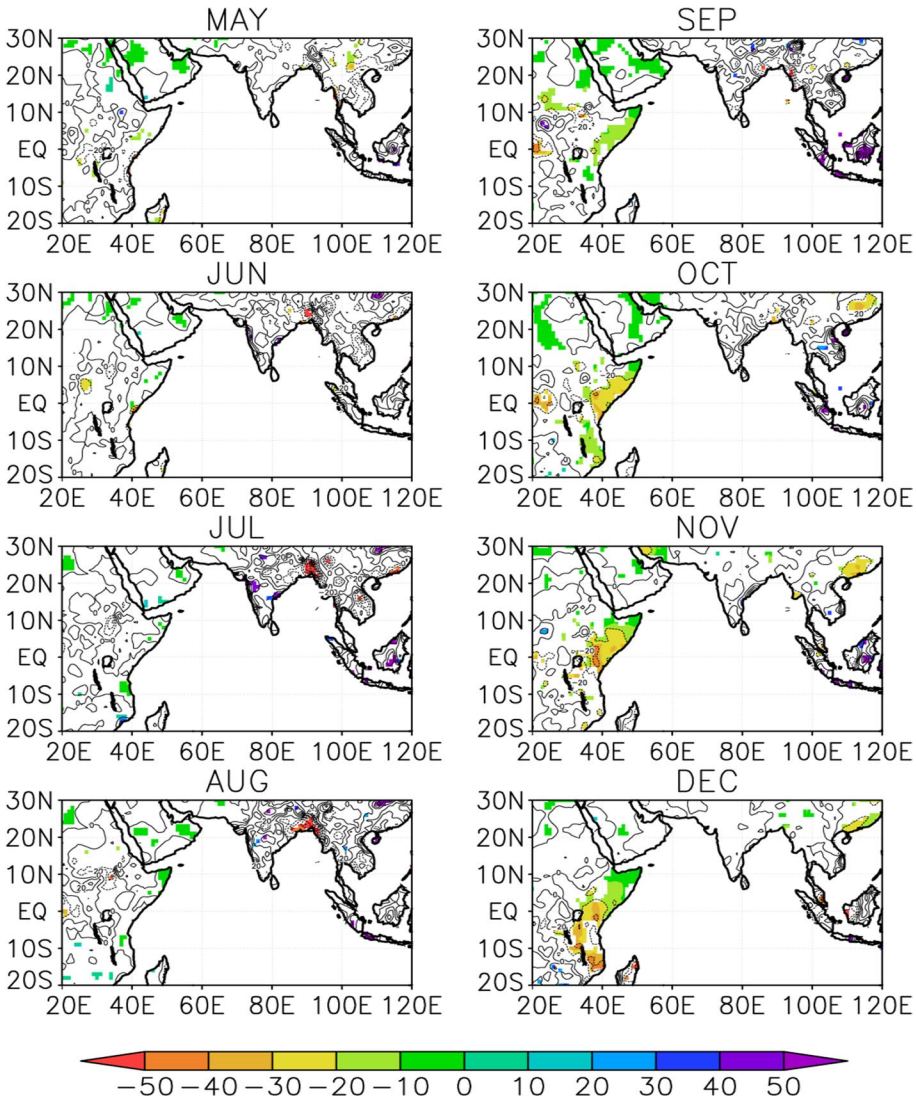

Fig. 14 As in Fig. 8, but for four negative canonical IOD events

In this study, we have succeeded in proposing a new classification method to distinguish different flavors of the IOD and described the main features of the two types of the IOD. The next step toward better understanding of these two types is quantitative discussion of how different SST anomaly patterns develop in the tropical Indian Ocean. Studies in this direction using an ocean general circulation model to calculate mixed layer temperature balance are under way.

Also, considering that there is a clear difference in impacts of the IOD on East Africa, which is vulnerable to anomalous rainfall and suffers from malaria outbreaks after heavy rainfall (Hashizume et al. 2009), this study suggests that it is important to predict not only an occurrence of an IOD event (Luo et al. 2007, 2008), but also its type. Assessing skills of coupled general circulation models to simulate and predict two types of the IOD is another important topic of future studies.

Finally, the relationship between the IOD and the Pacific Ocean has been discussed in many past studies (e.g., Ashok et al. 2003, 2004; Annamalai et al. 2005; Luo et al. 2010). Thus, it will be interesting to discuss the relationship between both types of the IOD and the Pacific. If there are any differences in the two types of the IOD, they may be

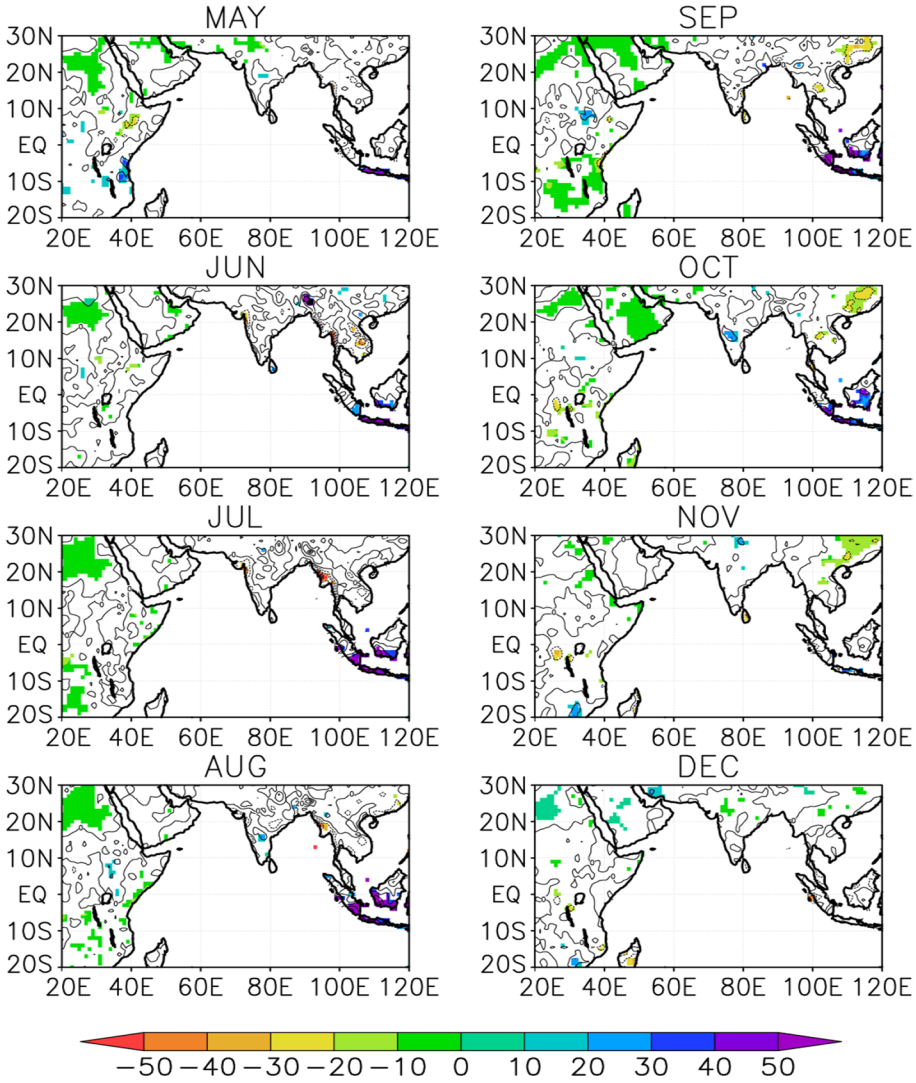

Fig. 15 As in Fig. 8, but for 10 negative IOD Modoki events

helpful to understand the relationship between the IOD and the Pacific. Further researches are needed to clarify their relationship using observational data and an ocean–atmosphere coupled model.

Acknowledgments We thank two anonymous reviewers for their constructive comments. The present research is supported by the Japan Science and Technology Agency, the Japan Agency for Medical Research and Development, and the Japan International Cooperation Agency through Science and Technology Research Partnership for Sustainable Development (SATREPS).

References

Adler RF et al (2003) The version 2 global precipitation climatology project (GPCP) monthly precipitation analysis (1979-present). J Hydrometeorol 4:1147–1167

Annamalai H, Xie SP, McCreary JP, Murtugudde R (2005) Impact of Indian Ocean sea surface temperature on developing El Niño. J Clim 18:302–319

Ashok K, Yamagata T (2009) The El Niño with a difference. Nature 461:481–484

Ashok K, Guan Z, Yamagata T (2003) A look at the relationship between the ENSO and the Indian Ocean Dipole. J Meteorol Soc Jpn 81:41–56

Ashok K, Guan Z, Saji NH, Yamagata T (2004) Individual and combined influences of ENSO and the Indian Ocean Dipole on the Indian summer monsoon. J Clim 17:3141–3155

Ashok K, Behera SK, Rao SA, Weng H, Yamagata T (2007) El Niño Modoki and its possible teleconnection. J Geophys Res 112:C11007. doi:10.1029/2006JCOO3798

Behera S, Yamagata T (2010) Imprint of the El Niño Modoki on decadal sea level changes. Geophys Res Lett 37:L23702. doi:10.1029/2010GL045936

Behera SK, Luo JJ, Masson S, Delecluse P, Gualdi S, Navarra A, Yamagata T (2005) Paramount impact of the Indian Ocean Dipole on the East African short rains: a CGCM study. J Clim 18:4514–4530

Behera S, Ratnam J, Masumoto Y, Yamagata T (2013) Origin of extreme summers in Europe: the Indo-Pacific connection. Clim Dyn 41:663–676

Behringer D, Xue Y (2004) Evaluation of the global ocean data assimilation system at NCEP: the Pacific Ocean. Preprint, Eighth

symposium on integrated observing and assimilation system for atmosphere, ocean and land surface, Seattle, WA, Am Meteorol Soc, 2.3. http://origin.cpc.ncep.noaa.gov/products/people/yxue/pub/13.pdf

Cai W, Cowan T, Raupach M (2009) Positive Indian Ocean Dipole events precondition southeast Australia bushfires. Geophys Res Lett 36:L19710. doi:10.1029/2009GL039902

Carton JA, Giese BS (2008) A reanalysis of ocean climate using simple ocean data assimilation (SODA). Mon Weather Rev 136:2999–3017

Du Y, Cai W, Wu Y (2013) A new type of the Indian Ocean Dipole since the mid-1970s. J Clim 26:959–972

Guan Z, Yamagata T (2003) The unusual summer of 1994 in East Asia: IOD teleconnections. Geophys Res Lett. doi:10.1029/2002GL016831

Hashizume M, Terao T, Minakawa N (2009) The Indian Ocean Dipole and malaria risk in the highlands of western Kenya. Proc Nat Acad Sci 106:1857–1962

Kalnay E et al (1996) The NCEP/NCAR 40-year reanalysis project. Bull Am Meteorol Soc 77:437–471

Kim ST, Yu JY (2012) The two types of ENSO in CMIP5 models. Geophys Res Lett 39:L11704. doi:10.1029/2012GL052006

Kim JS, Kim KY, Yeh SW (2012) Statistical evidence for the natural variation of the central Pacific El Niño. J Geophys Res 117:C06014. doi:10.1029/2012JC008003

Liebmann B, Smith CA (1996) Description of a complete (interpolated) outgoing longwave radiation dataset. Bull Am Meteorol Soc 77:1275–1277

Luo JJ, Masson S, Behera S, Yamagata T (2007) Experimental forecasts of Indian Ocean Dipole using a coupled OAGCM. J Clim 20:2178–2190

Luo JJ, Behera S, Masumoto Y, Sakuma H, Yamagata T (2008) Successful prediction of the consecutive IOD in 2006 and 2007. Geophys Res Lett 35:L14S02. doi:10.1029/2007GL032793

Luo JJ, Zhang R, Behera SK, Masumoto Y, Jin FF, Lukas R, Yamagata T (2010) Interaction between El Nino and extreme Indian Ocean Dipole. J Clim 23:726–742

McPhaden MJ, Lee T, McClurg D (2011) El Niño and its relationship to changing background conditions in the tropical Pacific Ocean. Geophys Res Lett 38:L15709. doi:10.1029/2011GL048275

Newman M, Shin SI, Alexander MA (2011) Natural variation in ENSO flavors. Geophys Res Lett 38:L14705. doi:10.1029/2011GL047658

Pourasghar F, Tozuka T, Jahanbakhsh S, Sari Sarraf B, Ghaemi H, Yamagata T (2012) The interannual precipitation variability in the southern part of Iran as linked to large-scale climate modes. Clim Dyn 39:2329–2341

Rao SA, Yamagata T (2004) Abrupt termination of Indian Ocean Dipole events in response to intraseasonal disturbances. Geophys Res Lett 31:L19306. doi:10.1029/2004GL020842

Rao SA, Behera SK, Masumoto Y, Yamagata T (2002) Interannual subsurface variability in the tropical Indian Ocean with a special emphasis on the Indian Ocean Dipole. Deep Sea Res II 49:1549–1572

Rao SA, Luo JJ, Behera SK, Yamagata T (2009) Generation and termination of Indian Ocean Dipole events in 2003, 2006 and 2007. Clim Dyn 33:751–767

Rayner NA, Parker DE, Horton EB, Folland CK, Alexander LV, Rowell DP, Kent EC, Kaplan A (2003) Global analysis of SST, sea ice and night marine air temperature since the late nineteenth century. J Geophys Res. doi:10.1029/2002JD002670

Saji NH, Yamagata T (2003) Possible impacts of Indian Ocean Dipole events on global climate. Clim Res 25:151–169

Saji NH, Goswami BN, Vinayachandran PN, Yamagata T (1999) A dipole mode in the tropical Indian Ocean. Nature 401:360–363

Smith TM, Reynolds RW, Peterson TC, Lawrimore J (2008) Improvements to NOAA's historical merged land-ocean surface temperature analysis (1880–2006). J Clim 21:2283–2296

Ummenhofer CC, England MH, McIntosh PC, Meyers GA, Pook MJ, Risbey JS, Sen Gupta A, Taschetto AS (2009) What causes southeast Australia's worst droughts? Geophys Res Lett 36:L04706. doi:10.1029/2008GL036801

Uppala SM, et al (2005) The ERA-40 re-analysis. Q J R Meteorol Soc 131 Part B:2961–3012

Weng H, Ashok K, Behera SK, Rao SA, Yamagata T (2007) Impacts of recent El Niño Modoki on dry/wet conditions in the Pacific rim during boreal summer. Clim Dyn 29:113–129

Xie PP, Arkin PA (1997) Global precipitation: a 17-year monthly analysis based on gauge observations, satellite estimates and numerical model outputs. Bull Am Meteorol Soc 78:2539–2558

Yeh SW, Kug JS, Dewitte B, Kwon MH, Kirtman BP, Jin FF (2009) El Niño in a changing climate. Nature 461:511–514

Yeh SW, Kirtman BP, Kug JS, Park W, Latif M (2011) Natural variability of the central Pacific El Niño event on multi-centennial timescales. Geophys Res Lett 38:L02704. doi:10.1029/2010GL045886